

Shape and Orbit Estimation Techniques for Space Debris Observation Using the Middle and Upper Atmosphere Radar (MU radar)

Naruomi Ikeda, Taiga Nishimura, Taiki Iwahori,
Mamoru Yamamoto, Hiroyuki Hashiguchi, and Hiroshi Yamakawa
Research Institute for Sustainable Humanosphere (RISH), Kyoto University

ABSTRACT

The aim of our study is to develop a method of estimating the shape and orbit of space debris using the Middle and Upper atmosphere (MU) radar, which is basically used for atmospheric observation. This can lead to an expansion of the observation network for space debris without constructing a new observation facility. In previous research using MU radar, the Single-Range Doppler Interferometry (SRDI) method had been proposed to estimate the shape of space debris. In the SRDI method, the shape of space debris can be estimated from a 2D imaging that uses the information of a fluctuating Doppler spectrogram caused by its spin motion. We will present results of the shape estimation of actual observations using the SRDI method. As for orbit estimation, we developed a technique to determine orbital elements of space debris from plural position vectors estimated from observation. We conducted actual observations using MU radar and succeeded in estimating the orbital plane with good accuracy. In this paper, the basic idea and some results for both shape and orbit estimations are presented.

1. INTRODUCTION

Recently, the amount of space debris has been observed to be rapidly increasing, which is becoming an obstacle for space exploration. Since the debris orbits the earth with high velocity, such as 7 to 8 km/s, it will cause severe damage to active satellites if they collide. Collisions also occur between pieces of space debris. Each collision generates new space debris, and thus the amount of space debris will continue to rapidly increase if remediation is not sought. Therefore, it is crucial to understand the space debris environment for sustainable space development. Currently, many organizations are observing space debris and storing such data. However, in 2009, there was a collision between an active communication satellite and satellite debris. The present observation network is not sufficient to completely avoid space accidents, and we need to improve and expand the observation network. As a means to expand the observation network, we propose an observation technique using atmosphere radar. Since atmosphere radar is already in use around the world, by applying this method, we can expand the observation network for space debris without constructing a new observation facility. Since atmosphere radar has poor range resolution compared to conventional radar for space debris observation, a special signal processing method must be developed. In order to confirm the effectiveness of our method, we made observations using the Middle and Upper atmosphere (MU) radar, which is a major observation facility in the Shigaraki MU Observatory of the Research Institute for Sustainable Humanosphere (RISH), Kyoto University. In section 2, we describe the characteristics of the MU radar. In sections 3 and 4, an overview of our shape estimation method and orbit estimation method is presented, respectively, and in section 5 we show results of shape and orbit estimations using MU radar. Section 6 is the conclusion.

2. CHARACTERISTICS OF THE MU RADAR

The MU radar is one of the largest atmosphere observation radar systems and can observe atmospheric motion and circulation between the troposphere (~2 km) and the upper atmosphere (~500 km) [1]. The most significant feature of the MU radar is that it can steer the radar beam direction at an extremely high speed of 2,500 times per second, by controlling high-power (2 kW) transmitter/receiver modules (475 units in total), each of which drives one antenna element. The MU radar has a circular antenna array with a diameter of 100 m, which can be divided into 25 subarrays to enable a space radar imaging observation. Fig. 1 shows a bird's-eye view of the MU radar, and Table 1 outlines the features of the MU radar.



Fig. 1 Bird's-eye view of the MU radar

Table 1 Specifications of the MU radar

Location of the observatory	Shigaraki-cho, Koga-city, Shiga, Japan (34°51' N, 136°06' E)
Operational frequency	46.5 MHz
Occupied frequency bandwidth	3.5 MHz
Antenna	475 elements of crossed Yagi antennas
Structure	Circular antenna array with a diameter of 103 m
Functions	Electronic beam steering
Beam width	3.6° (half-power full width)
Transmission output power	1 MW (peak)

3. SHAPE ESTIMATION TECHNIQUE

This section presents an overview of our shape estimation method. Since MU radar has large-range resolution (a few km), it is difficult to use information on range direction for a shape estimation. Hence, we apply the Single-Range Doppler Interferometry (SRDI) method [2, 3]. The SRDI method uses Doppler frequency caused by rotation of the target, and creates a 2D image and estimates the shape. Fig. 2 shows the scheme of the SRDI method. Assuming a scatterer that is rotating with a radius of r and angular frequency of ω (see Fig. 3), then the Doppler angular frequency generated from the rotating scatterer is given by the differential of the phase of the signal, expressed by Eq. 1:

$$\omega_d(\theta) = -\frac{4\pi\omega}{\lambda}r \cos(\theta + \theta_0) \quad (1)$$

where λ is the wavelength of the radar and θ_0 is the initial phase of the scatterer. As evident from Eq. 1, the Doppler frequency is the sine function of time, and its amplitude contains information on the size and rotation rate of the target. Therefore, we can estimate the size of the target by analyzing the temporal fluctuation of the Doppler frequency.

In order to obtain the temporal change of the Doppler frequency, we use the time-frequency analysis method called Smoothed Pseudo Wigner-Ville Distribution (SPWD). The most frequently used time-frequency analysis should be Short-Time Fourier Transform (STFT); however, there is another method that has better time-frequency resolution than the STFT, called Wigner-Ville Distribution (WVD). WVD can be expressed as Eq. 2:

$$S_{WVD}(t, \omega) = 2 \int s(t + \tau) s^*(t - \tau) e^{-j\omega\tau} d\tau \quad (2)$$

where $s(t)$ is the complex time series signal obtained from the radar, and $s^*(t)$ is the complex conjugate of $s(t)$. WVD can obtain high time-frequency resolution; however, if the signal contains multiple frequencies, WVD will acquire a virtual image caused by interferences of adjacent frequencies. In order to solve this problem, it is effective to use SPWD, given by the following equations:

$$S_{SPWD}(t, \omega) = \int \int \Phi(t - t', \omega - \omega') S_{WVD}(t', \omega') dt' d\omega' \quad (3)$$

$$\Phi(t, \omega) = \exp\left(-\frac{t^2}{\alpha^2} - \frac{\omega^2}{\beta^2}\right), \quad (4)$$

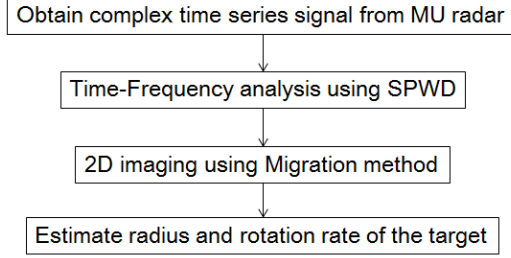


Fig. 2 Scheme of the SRDI method

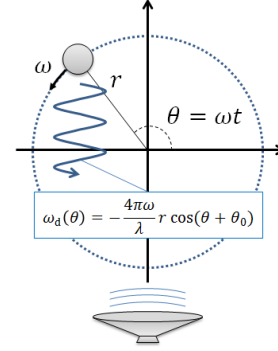


Fig. 3 Rotating scatterer

In Eq. 4, $\Phi(t, \omega)$ is the smoothing function. We can obtain the temporal change of the Doppler function with high time-frequency resolution by selecting appropriate α and β in Eq. 4.

Next, we apply the Migration method on the SRDI method [4]. First, using the result of SPWD and the relation shown in Eq. 1, we can convert the spectrogram $S(t, \omega)$, which is the function of time and frequency, into the function of radius and angle, $S(r, \theta)$. Then, the spectrogram $S(r, \theta)$ can be smoothed using Eq. 5.

$$S_{\text{Migration}}(r, \theta) = \frac{1}{2\pi} \int_0^{2\pi} S(r \cos\{\theta' - \theta\}, \theta') d\theta' \quad (5)$$

Eq. 5 indicates the line integral along the circle that passes through the origin (0,0) and arbitrary point (r, θ) . The target is likely to be at the point which has power spectral density ($S_{\text{Migration}}$) over a certain threshold. Hence, we can estimate the shape of the target from this 2D imaging. Note that before applying Migration, we need to estimate angular frequency ω by analyzing the differential of the phase.

4. ORBIT DETERMINATION TECHNIQUE

This section provides an overview of our orbit estimation method. Fig. 4 indicates the scheme of our orbit determination method. First, acquire the time series signal from multiple beams using MU radar, and then calculate the distance and direction at each time. Finally, estimate the orbit of the target using the temporal change of the position, as calculated above.

The MU radar can obtain echoes from different heights depending on its observation parameters such as pulse transmission interval, range resolution, and so on. Now we assume that we obtained echoes from N regions, and the region number that has the strongest echo is n ($1 \leq n \leq N$). Then the distance between the target and the radar can be calculated using Eq. 6:

$$r = h_{\min} + \frac{(n + \Delta)c_0\tau}{2} \quad (6)$$

$$\Delta = \begin{cases} \frac{1 - \frac{a}{b}}{2} & (a < b) \\ \frac{\frac{b}{a} - 1}{2} & (a \geq b) \end{cases} \quad (7)$$

where h_{\min} is the minimum distance of the observation, c_0 is the speed of light, and τ is the pulse width. Δ is the correction term expressed as Eq. 7, where a is the difference between the maximum signal intensities of n and $n + 1$ region, and b is the difference between n and $n - 1$ region.

As the direction estimation method, we applied the Sequential Beam Lobing method [5]. This method uses the difference between the echo strength of three beams to estimate the direction of the target. For example, if two beams in different directions have beam echoes with the same strength, this means that the target is located at the center of these beams (Fig. 5a).

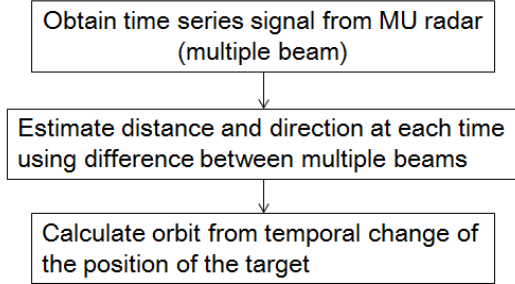


Fig. 4 Scheme of the Orbit determination

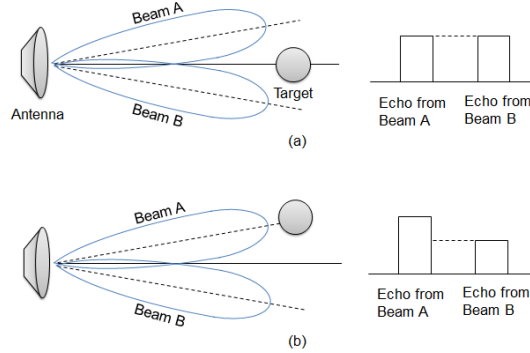


Fig. 5 Example of Sequential Beam Lobing

If there is a difference between them, the target is located in the direction of the stronger beam echo (Fig. 5b). By performing this calculation with two pairs of beams, we can estimate the direction of the target. Using the distance and direction of the target at each time, we can obtain the time change of the position of the target. Assume that we obtain n positions of the target from $t = t_1$ to t_n , and express it as (x_i, y_i, z_i) ($i = 1, \dots, n$). Then find the orbit that will match these observed points using the Gauss-Newton method [6], which is a basic method to solve the non-linear least-squares method. First, calculate the initial value of fitting parameter $\beta = (X, Y, Z, V_x, V_y, V_z)$, where (X, Y, Z) is position and (V_x, V_y, V_z) is velocity, using the Herrick-Gibbs method [7]. The Herrick-Gibbs method is used to calculate velocity from the position of three consecutive points. To obtain the results shown in the following section, we used three points around the zenith obtained from the observation. Using β , we can calculate the Two-Line Elements (TLEs), which are the parameters that express the shape of the orbit, such as inclination, semi-major axis, eccentricity, and so on. Then we calculate the temporal change of the position predicted from the TLEs calculated from β , and express it as (X_i, Y_i, Z_i) ($i = 1, \dots, n$). Finally, we perform the optimization using the Gauss-Newton method, expressed by Eq. 8 to Eq. 11, and determine the β that will minimize the error between the time change of the position of the observed value and the calculated orbit:

$$S(\beta) = \sum_{i=1}^n r_i(\beta) \quad (8)$$

$$r_i(\beta) = \sqrt{(x_i - X_i)^2 + (y_i - Y_i)^2 + (z_i - Z_i)^2} \quad (9)$$

$$\beta^{(s+1)} = \beta^{(s)} - (J_r^T J_r)^{-1} J_r^T r(\beta^{(s)}) \quad (10)$$

$$J_r = \frac{\partial r_i(\beta^{(s)})}{\partial \beta_j} \quad (11)$$

5. ESTIMATION RESULTS

This section describes the results of both shape and orbit estimations. For shape estimation, we made an observation of H-2A rocket body debris (NORAD ID: 27601U) on January 10, 2017, using MU radar. Fig. 6 shows the image of the second rocket stage of the H-2A rocket, and Table 2 indicates the observation parameters. As for orbit estimation, we made observations of OAO-3 satellite debris (NORAD ID: 06153U), which is also observed on January 10, 2017. Fig. 7 shows the image of the OAO-3 satellite, and Table 3 indicates the observation parameters. It was predicted that the OAO-3 pass over the MU radar twice a day, we made two observations against OAO-3. The biggest difference in the observation parameters is the beam number; we used ten beams along the orbit for the orbit

estimation, since our orbit determination method needs at least three beams to estimate the position of the target. As for shape estimation, we only used two beams at closer point for the observation. It seems to be effective to use multiple beams for shape estimation; however, there is a trade-off between beam number and the observation time interval. We chose to use two beams in order to have a sufficient time resolution.

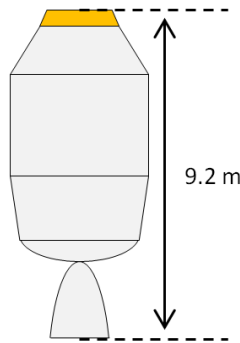


Fig. 6 Image of the H-2A rocket body [8]

Table 2 Observation parameters for H-2A

Range resolution	4,800 m
Total number of height regions	40
Pulse width	32 μ s
Minimum height	690 km
Interpulse period	8,320 μ s
Beam direction (azimuth, zenith)	(100,5), (105,5)



Fig. 7 Image of the OAO-3 satellite [9]

Table 3 Observation parameters for OAO-3

Range resolution	4,800 m
Total number of height regions	80
Pulse width	32 μ s
Minimum height	600 km
Interpulse period	8,320 μ s
Beam direction (azimuth, zenith)	(0,0), (120,2), (180,2), (240,2), (85,8), (100,8), (265,8), (250,8), (90,10), (255,10)

5.1 SHAPE ESTIMATION

In this subsection, shape estimation results of the H-2A rocket body are presented. Fig. 8 shows the result of time-frequency analysis using SPWD. According to the discussion in section 3, the Doppler frequency generated from a rotating object should be a periodic function; however, Fig. 8 shows a linear change of the Doppler frequency, which wraps at the Nyquist frequency. We consider this is to be due to the strong change of the phase caused by the orbital motion of the target, since space debris is orbiting at a few km/s and has a large relative velocity to the radar. We removed this effect by canceling the tilt shown in Fig. 8, in order to extract the Doppler frequency. The result of SPWD after removing orbital effect is shown in Fig. 9. After that, we also applied the High-Pass Filter (HPF), because there was a strong echo around 0 Hz, which is caused by the strong echo from the center of the rotation. Fig. 10 shows the result of SPWD after removing the orbital effect and applying HPF. We can see the periodic change of the Doppler frequency from Fig. 10. Before applying the Migration method, we have to estimate the angular frequency of the target. This can be achieved by analyzing the frequency of the differential of the phase, because the Doppler angular frequency is defined by the time differential of the phase of the signal. Fig. 11 shows the result of the Fourier transform of the time differential of the phase. From Fig. 11 we can estimate the rotation frequency as $f_0 = 0.3$ [Hz] ($\omega_0 = 1.88$ [rad/s]). Note that if the target is symmetric, the actual rotation rate is half of this value. Therefore, we assume two cases for Migration. Finally, we applied the Migration method and the results of symmetric and asymmetrical cases are shown in Fig.12 and Fig.13, respectively. We concluded that the rotation radius is 0.50 m (symmetric) or 0.75 m (asymmetric). However, the true size of the second rocket stage of H-2A is 4.6 m in radius, and both estimation results are smaller than this value. Possible reasons for this difference is an error

in definition of spectral power density threshold, or the strong echo from the middle of the rocket body instead of the edge of the rocket body. For improvement, we are going to use other information such as temporal change of the radar cross section, or use multiple beams for analysis.

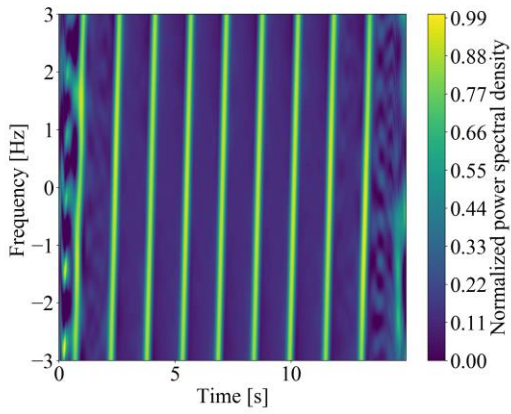


Fig. 8 Simple SPWD

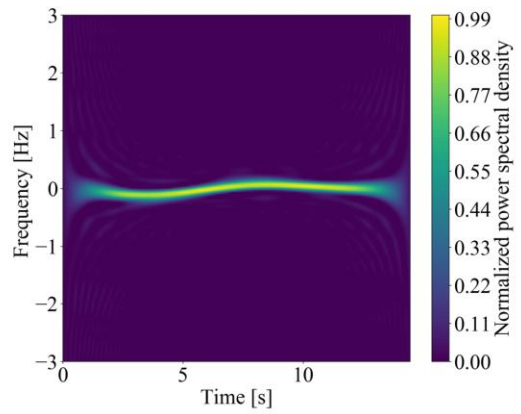


Fig. 9 SPWD without orbital effect,

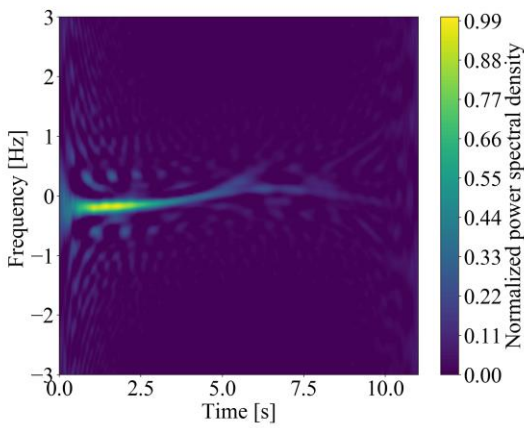


Fig. 10 SPWD without orbital effect, and applying HPF

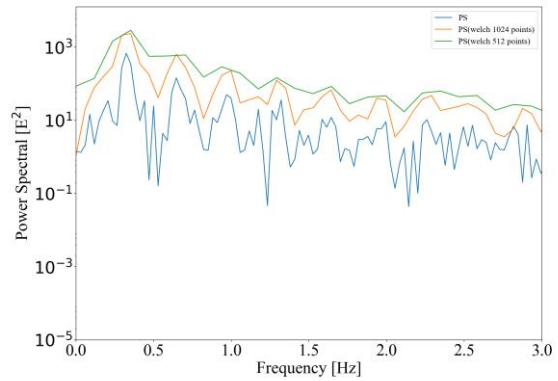


Fig. 11 Differential of the phase

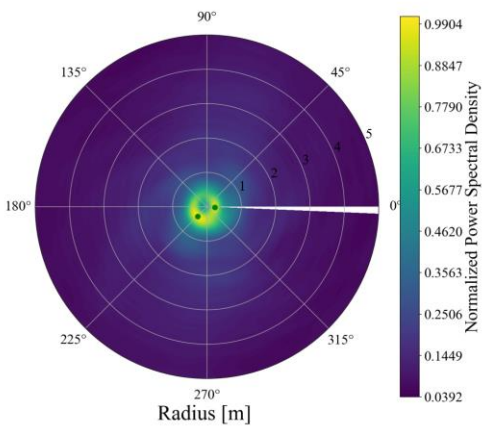


Fig. 12 Migration result (symmetric)

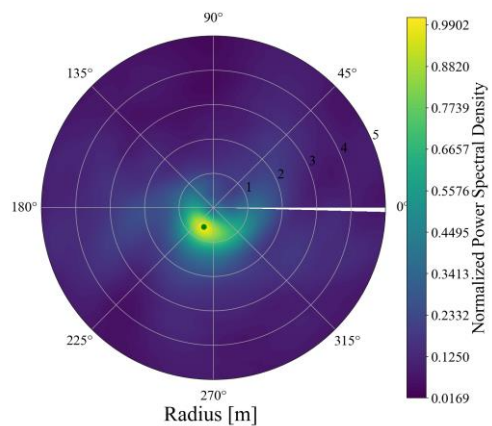


Fig. 13 Migration result (asymmetric)

5.2 ORBIT ESTIMATION

In this subsection, orbit estimation results of OAO-3 satellite debris are presented [10]. Fig. 14 to Fig. 19 shows the results of first observation. Fig. 14 shows the beam distribution for this observation. The blue line is the orbit predicted from TLE, and the red points indicate the beam positions; we used 10 beams for this observation. Fig. 15 shows the echoes from different heights of beam 6. Using these values and Eq. 6, we can calculate the temporal change of the distance as Fig. 16. The solid purple line indicates the distance change predicted from TLE, and black points show the results from the observation. We succeeded in estimating the temporal change of the distance with an error less than 1 km. Fig. 17 shows the echoes from beams 0 to 3 (located around the zenith). From these values, the temporal change of the zenith angle and the azimuth angle can be calculated as Fig. 18 and Fig. 19. Both the zenith angle and azimuth angle showed good correspondence. We succeeded in estimating the change of zenith and azimuth angles with less than 0.1 degree error. Finally, Table 4 shows the comparison of the estimated TLEs with true values. Estimation 1 uses only the data from first observation, and Estimation 2 uses data from both first and second observations. Results shows that even one time observation, the estimation results of parameters which define the orbital plane (i, Ω) had good accuracy. Accuracy of less than 0.1 degrees was achieved using data spanning 20 seconds. In addition, when we perform observation twice, the estimation accuracy of parameters which defines size of the orbit (e, n) significantly improved. However, there is still some error in parameters for orbit size. This comes from the error in the distance determination, because i and Ω only use information of the azimuth and zenith angles, and e and n are calculated using information on distance, which had an error as shown in Fig. 16. This error is likely caused by the large-range resolution of MU radar, but we aim to improve the distance estimation in future work.

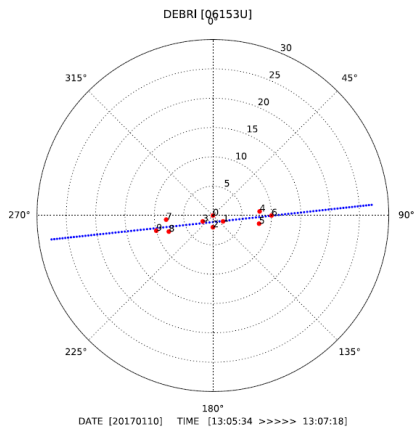


Fig. 14 Predicted orbit of OAO-3

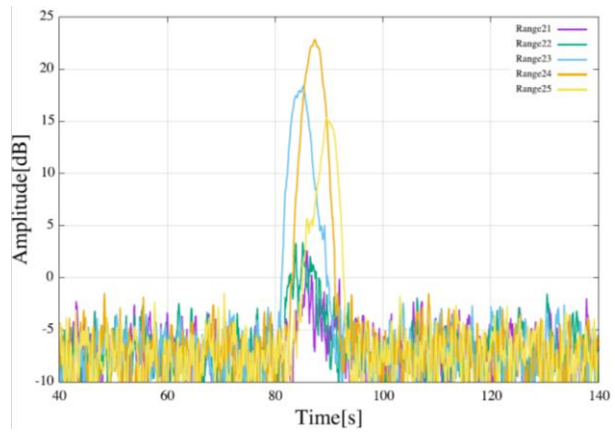


Fig. 15 Echoes from different heights of beam 6

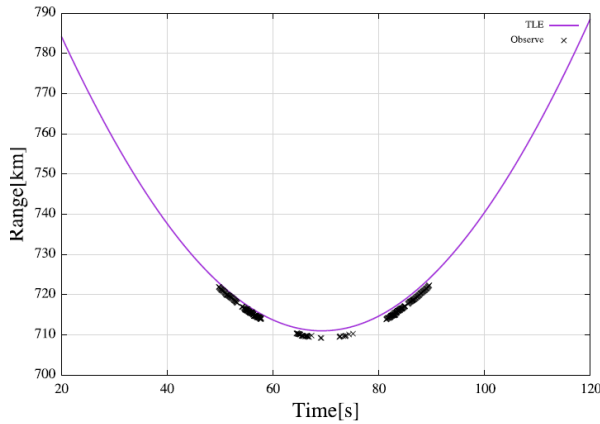


Fig. 16 Comparison of observed/predicted distance

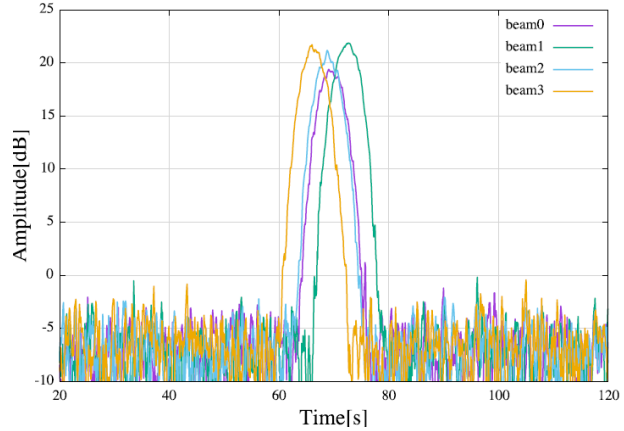


Fig. 17 Echoes from different beams

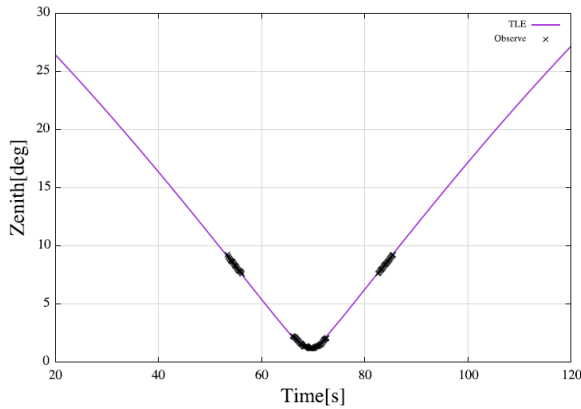


Fig. 18 Comparison of observed/predicted zenith

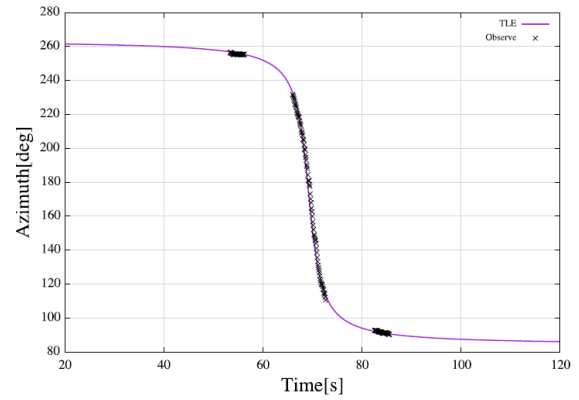


Fig. 19 Comparison of observed/predicted azimuth

Table 4 Comparison of estimated TLE and true values

TLE	Inclination i [deg.]	Right ascension of the ascending node Ω [deg.]	Eccentricity e	Argument of perigee ω [deg.]	Mean anomaly M [deg.]	Mean motion n
True value	35.01	227.76	0.0007	226.54	214.40	14.58
Estimation 1	34.96	227.11	0.0185	70.63	10.23	14.16
Estimation 2	35.05	228.63	0.0152	180.57	260.22	14.56

6. CONCLUSION

This paper presents the basic idea of shape and orbit estimations of space debris using MU radar. We performed shape estimation of H-2A rocket body debris, and estimated the angular frequency and the radius of the rotation. However, the estimation result was smaller than the actual size of the H-2A rocket body. We consider this to be due to the error in spectral density threshold, or the strong echo from the middle of the rocket body instead of the edge. We are going to address this problem using other information, such as temporal change of the radar cross section, or multiple beam analysis, in an attempt to improve estimation accuracy. We also performed the orbit estimation of OAO-3 satellite debris, and succeeded in estimating parameters that define the orbital plane with high accuracy by one time observation of 20 seconds. When we performed second observation for same debris and estimated the orbit using data from both observations, the estimation accuracy of parameters which defines the orbit size showed significant improvement. However, there is still some estimation error in parameters for the size of orbit. We consider this to be caused by the error in the distance estimation, and we will attempt to improve the distance estimation in future work.

7. ACKNOWLEDGEMENTS

This work is adopted as the MU radar and Equatorial Atmosphere Radar (EAR) collaboration research, and supported by JSPS KAKENHI Grant number 15K06600.

8. REFERENCES

1. Research Institute for Sustainable Humanosphere, Kyoto University. Retrieved from <http://www.rish.kyoto-u.ac.jp/mu/en/detail.html>.
2. Toru Sato. "Shape estimation of space debris using single-range Doppler interferometry." *IEEE Transactions on Geoscience and Remote Sensing* 37.2 (1999): 1000-1005.
3. Atsuhito Kawahara, Taiki Iwahori, Hiroshi Yamakawa, Toru Sato, Mamoru Yamamoto, and Hiroyuki Hashiguchi. "Study on Space Debris Observation Method Using Kyoto University MU Radar." *Journal of the Japan Society for Aeronautical and Space Sciences* 64.3 (2016): 189-199 (in Japanese).
4. Milton Burnett Dobrin. *Introduction to Geophysical Prospecting*. McGraw-Hill, 1976.
5. Bassem R. Mahafza. *Radar Systems Analysis and Design Using MATLAB*. CRC Press, 2002.
6. Dimitri P. Bertsekas. *Nonlinear Programming*. Belmont: Athena Scientific, 1999.
7. Andrew Vernon Schaeperkoetter. *A Comprehensive Comparison Between Angles-only Initial Orbit Determination Techniques*. Diss. Texas A&M University, 2012.
8. JAXA | H2A Launch Vehicle. Retrieved from <http://global.jaxa.jp/projects/rockets/h2a/>.
9. NASA—NSSDCA—Spacecraft—Details. Retrieved from <https://nssdc.gsfc.nasa.gov/nmc/spacecraftDisplay.do?id=1972-065A>.
10. Taiga Nishimura. "Orbit Determination Technique Exploiting MU Radar." Master's thesis, Kyoto University, 2017 (in Japanese).